



# Improvement of critical parameters of $\text{YBa}_2\text{Cu}_3\text{O}_{6.9}$ by low temperature treatment in the presence of water vapors



I.B. Bobylev\*, E.G. Gerasimov, N.A. Zyuzeva

M.N. Miheev Institute of Metal Physics, Ural Branch of the Russian Academy of Sciences, S. Kovalevskaya St., 18, Yekaterinburg 620990, Russia

## ARTICLE INFO

### Article history:

Received 28 April 2015

Received in revised form 10 August 2015

Accepted 24 August 2015

Available online 1 September 2015

### Keywords:

Y–Ba–Cu–O

Critical parameters

Low temperature treatment

Water vapor

## ABSTRACT

The effect of double thermal treatment at temperatures of 200 °C and 930 °C on the critical parameters of highly textured  $\text{YBa}_2\text{Cu}_3\text{O}_{6.9}$  ceramics has been examined. It has been shown that particles non-superconducting at  $T = 77$  K, as well as planar stacking faults formed at low-temperature treatment in a humid atmosphere, are pinning centers of magnetic vortices. After recovery annealing (at 930 °C), the planar faults are partially preserved and serve as effective pinning centers in a magnetic field perpendicular to the *c*-axis. In addition, optimal double-annealing conditions have been found to significantly increase the critical current density up to the values  $j_c \geq 10^4$  A/cm<sup>2</sup> in the external magnetic field (10 T), applied perpendicular to the *c*-axis.

© 2015 Elsevier Ltd. All rights reserved.

## 1. Introduction

It is known [1–3] that the creation of nanoscale structural inhomogeneities, which differ in their chemical composition and properties from the matrix superconducting phase, leads to reinforcement of pinning of magnetic vortices. This provides higher current-carrying capacity of HTS (high temperature superconductors) – materials in high magnetic fields, which is important for practical applications [4]. There are different ways to create the pinning centers. One of them is the injection of complex oxides such as  $\text{Y}_2\text{BaCuO}_5$  [5],  $\text{BaZrO}_3$  [6,7],  $\text{BaSnO}_3$  [8], and some titanates and niobates [9,10]. On the other hand, the heat treatment method may be also effective to raise the density of native structural defects [11,12].

In the Refs. [13,14], it was found that during the thermal treatment of  $\text{YBa}_2\text{Cu}_3\text{O}_y$  (123) ( $y = 6.5$ – $6.8$ ) compounds at 200 °C, the formation of particles of 5–10 nm size close to the coherence length ( $\xi \sim 1.5$  nm) due to the phase decomposition occurs. The particles formed have a low oxygen index ( $y \sim 6.1$ ) [15] and exhibit no superconductivity at  $T = 77$  K. The assumption was made that such particles may produce the pinning of magnetic vortices.

In contrast to the foregoing paragraph, the paper [16] claims that the  $\text{YBa}_2\text{Cu}_3\text{O}_y$  compound interacts with atmospheric moisture at temperatures near room temperature, where by the 124-type stacking faults arise. These defects involve extra Cu–O layers with the length of  $\sim 20$  nm and the thickness of

1.2–2.4 nm. In the books [17–20], it is shown that the oxygen non-stoichiometric 123-type interacts with atmospheric moisture even at higher temperatures ranging from 100 °C to 300 °C. The authors of the above works suppose that its structure contains water in the form of  $\text{OH}^-$ -groups, which cause the formation of the 124-type planar defects. In [21], it was discovered by the TEM-method that the stacking fault packets are formed inside the 123-type when annealing the latter at 200 °C in a humid atmosphere. In the case of prolonged treatment under these conditions, the  $\text{YBa}_2\text{Cu}_3\text{O}_y$  compound passes into the non-superconducting phase of the pseudo 124-type [18]. A study in [22] concludes that after water absorption  $\text{YBa}_2\text{Cu}_3\text{O}_{6.8}$  shows antiferromagnetic fluctuations, which are not inherent in the 123-type with a high oxygen content.

In [23,24], ceramic samples of the 123-type were examined after treatment at 200 °C in a humid atmosphere and after recovery annealing at 930 °C followed by oxidation at 400 °C. The recovery annealing is required for ceramic sintering and removing the excess of structural defects. It is shown that such integrated annealing noticeably improves the field dependence of the critical current density ( $j_c$ ) as compared with the initial state.

In this paper, we have investigated how the critical characteristics of the high-textured  $\text{YBa}_2\text{Cu}_3\text{O}_{6.9}$  ceramics are affected by low-temperature annealing in atmospheres with different humidity, by a natural aging process and recovery annealing at 930 °C. The objective of this research is to determine the dependencies of the critical characteristics on water content inside the samples and optimize the annealing conditions in order to improve greatly the current-carrying capacity of advanced materials such as

\* Corresponding author. Tel.: +7 3433783667.

E-mail address: [bobylev@imp.uran.ru](mailto:bobylev@imp.uran.ru) (I.B. Bobylev).

123-type, which makes them promising for many practical applications.

**2. Experimental technique**

A material to study was  $YBa_2Cu_3O_{6.9}$  ceramics, synthesized by the MTG-method (the melt-textured growth method) [25,26] at the A.A. Bochvar High-Technology Scientific Research Institute for Inorganic Materials. The X-ray analysis showed that the *ab*-plane reflected 001 lines only, which indicates a high texture of the material. The samples contained 30 wt.%  $Y_2BaCuO_5$  (211). Besides, many of the investigations were conducted on single crystals, obtained by the solution-melt method. [27].

Low temperature treatment had been carried out for 5–300 h at 200 °C in an oxygen atmosphere or argon saturated with water vapor. Recovery annealing was performed at 930 °C (1 h) in an air atmosphere followed by oxidation at 400 °C in the oxygen atmosphere (24 h) to achieve the oxygenation index  $\approx 6.9$ . In addition, a sample aged for about 15 years was investigated under normal conditions and natural moisture. It was found that the sample absorbed  $\sim 0.1$  wt.% water.

Magnetization measurements were taken at  $T = 77$  K in pulsed magnetic fields. Bipolar pulse duration amounted to  $\sim 7.5$  ms. The maximum amplitude of pulsed magnetic induction was equal to 35 T, with the charging voltage of a capacitor bank being 2500 V. Magnetization of some samples was also investigated using a vibrating magnetometer in quasi-static magnetic fields with induction of up to 1.5 T. The magnetization values obtained by the vibrating magnetometer were close to the appropriate values obtained in the pulsed magnetic fields with the pulse amplitude  $B = 3\text{--}4$  T (Fig. 1). Moreover, we have conducted an investigation concerning the dependence of the magnetization loop width ( $\Delta M$ ) in a zero field on the rate of change of the magnetic flux density. As is seen from Fig. 2, the values of  $\Delta M$  at the rate of  $\sim 500$  T/s (it corresponds to the maximal induction of  $\sim 3.5$  T) exceed the appropriate values obtained in the quasi-static field only by 10–15%. These are consistent with data from Refs. [28,29]. Also, it has been found that the rate of change of the magnetic induction almost never affects the irreversibility field values ( $H_{irr}$ ).

With the maximum magnetic field of 35 T, the magnetization loop width significantly increased as compared to the width measured in the fields with the maximum induction  $B = 4$  T. Therefore, calculating the critical current density in the fields of  $>4$  T, we have reduced the magnitudes of  $\Delta M$  to the appropriate values

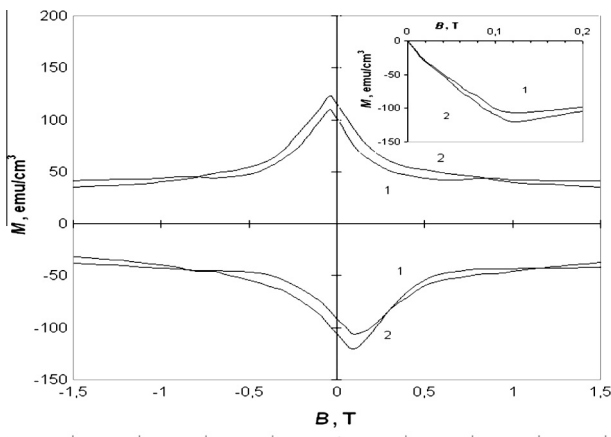


**Fig. 1.** Dependencies of the magnetization of the original sample in the field applied  $\perp c$ . The results are obtained using a vibration (1) and pulsed (2) magnetometer at the rate of change of the magnetic flux density of 500 T/s. The inset shows the initial segments of the curves.

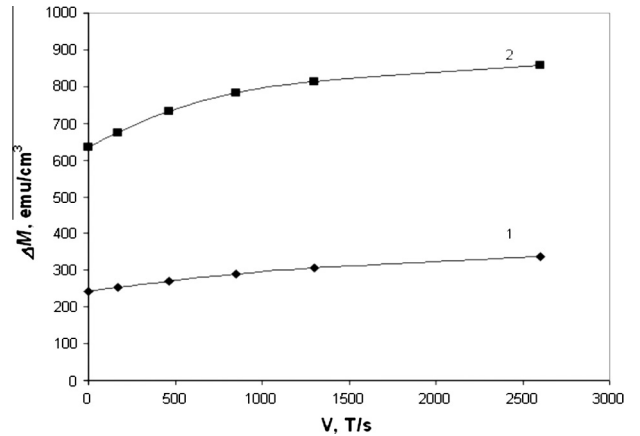


**Fig. 2.** Dependencies of the magnetization loop width ( $\Delta M$ ) in a zero field on the rate of changes of the magnetic induction: (1) the field is applied  $\parallel c$  and (2) the field is applied  $\perp c$ .

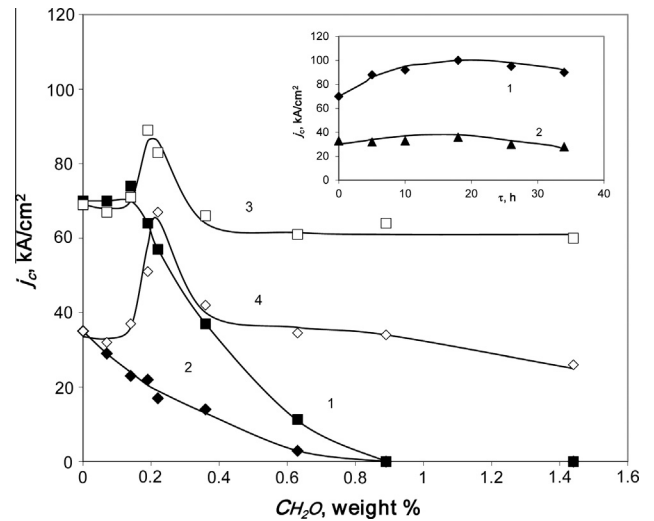


**Fig. 3.** Critical current densities ( $T = 77$  K) versus water content in the samples heat treated at 200 °C (1 – in the field parallel to  $c$ ; 2 – in the field perpendicular to  $c$ ) and after annealing at 930 °C followed by oxidation (3 –  $\parallel c$ ; 4 –  $\perp c$ ). Inset: dependences of the critical current density on the time of 200 °C annealing in oxygen atmosphere (1 –  $\parallel c$ ; 2 –  $\perp c$ ).

obtained in the fields of  $<4$  T. Thus the results obtained by us can be inflated no more than 10–15%.

The hysteresis loops were taken in the field imposed both parallel to the *c*-axis ( $\parallel c$ ) and perpendicular to it ( $\perp c$ ). The samples were sawn from one portion of the block of the highly textured ceramics with a uniform macrostructure and had the following dimensions  $\cong 2.5 \times 2.5 \times 1.5$  mm. The critical current density was calculated using the modified Bean formula [30]

$$j_c = 20\Delta M/a(1 - a/3b),$$

where  $\Delta M$  is the magnetization loop width ( $\text{emu}/\text{cm}^3$ );  $a$  and  $b$  are the dimensions of the rectangular sample (cm,  $a < b$ ). The pinning force  $F_p$  was estimated according to the equation:

$$F_p = j_c \cdot B.$$

The values of the lower critical field ( $B_{c1}$ ) were determined by the deviation from the linear dependence of the initial part of the curve  $M = f(B)$ . The hysteresis loops with a maximum amplitude of the magnetic field induction of  $B \sim 3$  T were used to determine  $B_{c1}$ .

To control the water content in the samples treated at 200 °C in a humid atmosphere, we used a gravimetric method [15]. The mass measurement error was  $\pm 0.005\%$ . X-ray examination was made using a diffractometer of DRON-3M type with copper radiation (Cu  $K\alpha$ ). For optical investigation of the single crystals, we utilized a polarized light microscope of Neofot-32 type. Temperature dependences of the magnetic susceptibility were measured on a Quantum D MPMS XL5 type SQUID magnetometer at a frequency of 80 Hz and at alternating field amplitude of 4 Oe.

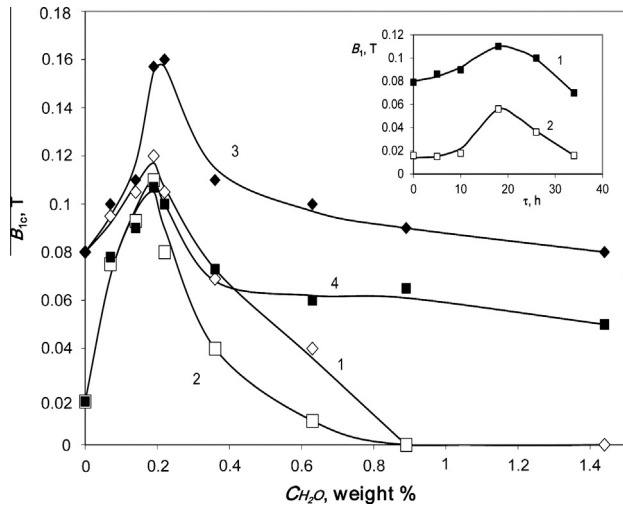


**Fig. 4.** Lower critical fields ( $B_{c1}$ ) ( $T = 77$  K) versus water content in the samples heat treated at 200 °C (1 –  $\parallel c$ , 2 –  $\perp c$ ) and after annealing at 930 °C followed by oxidation (3 –  $\parallel c$ , 4 –  $\perp c$ ). Inset: dependences of  $B_{c1}$  on the time of 200 °C annealing in oxygen atmosphere (1 –  $\parallel c$ , 2 –  $\perp c$ ).

### 3. Results and discussion

The dependencies of  $j_c$  in low fields ( $B \approx 0$  T) on the samples' water concentration are plotted in Fig. 3. As can be seen from the figure, the values of  $j_c$  decrease in both orientations of the applied field (Fig. 1, curves 1, 2) as the water content increases. However, similar dependencies  $B_{c1} = f(C_{H_2O})$  have distinct maxima after  $\sim 0.2$  wt.% water absorption (Fig. 4, curves 1, 2), with the maximum values of  $B_{c1}$  being approximately the same ( $\sim 0.11$  T). Apparently, the planar defects formed inhibit the penetration of the magnetic field, especially along the  $\perp c$ -direction.

As a comparison, we give the results obtained by us in [31]: after annealing of 123 at a temperature of 200 °C in an oxygen atmosphere for  $\approx 20$  h,  $j_c$  also grows appreciably (Fig. 3, shown in the inset). The dependencies  $B_{c1} = f(\tau)$  also have peaks at  $\tau = 20$  h (Fig. 4, shown in the inset). According to the gravimetric data, there is almost no water absorption (0.02 wt.% for 40 h of annealing) during the annealing process in the oxygen atmosphere. It can be assumed that under oxidizing medium, only the decomposition of the  $YBa_2Cu_3O_y$  compound into phases with different oxygen contents takes place.

The state diagram of  $YBa_2Cu_3O_6 - YBa_2Cu_3O_7$  [32] indicates that non-superconducting particles with low oxygen content are precipitated as the phase decomposition of  $YBa_2Cu_3O_y$  ( $y \geq 0.5$ ) occurs. These particles may serve as pinning centers, but too large a number of them can lead to the degradation of the critical parameters. The maxima on the curves  $j_c = f(\tau)$  and  $B_{c1} = f(\tau)$  appear to be associated with the precipitation process of optimal quantity of the non-superconducting particles when treating the samples in a dry atmosphere.

As has been noted above, when the samples absorb water, the stacking fault packets having substantially larger sizes compared to the particles precipitated are formed. Also, around them stress fields of opposite signs appear. With the optical microscope, the

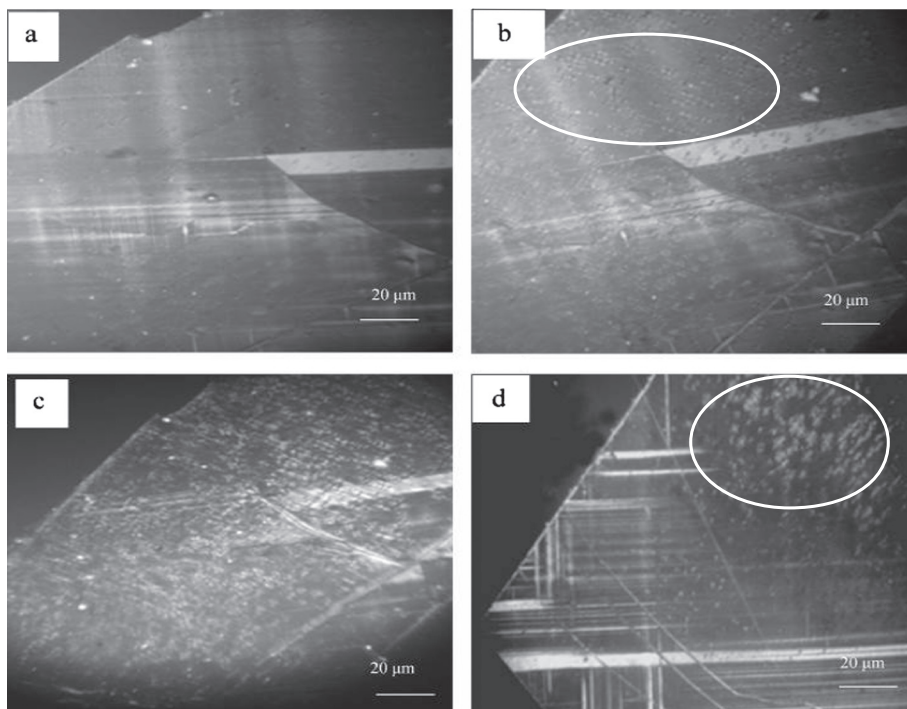


**Fig. 5.** Micrographs of  $YBa_2Cu_3O_{6.9}$  single crystal in the initial state (a); heat treated at 200 °C, 20 h (b); heat treated at 200 °C, 100 h (c) and after room temperature ageing for about 15 years (d).

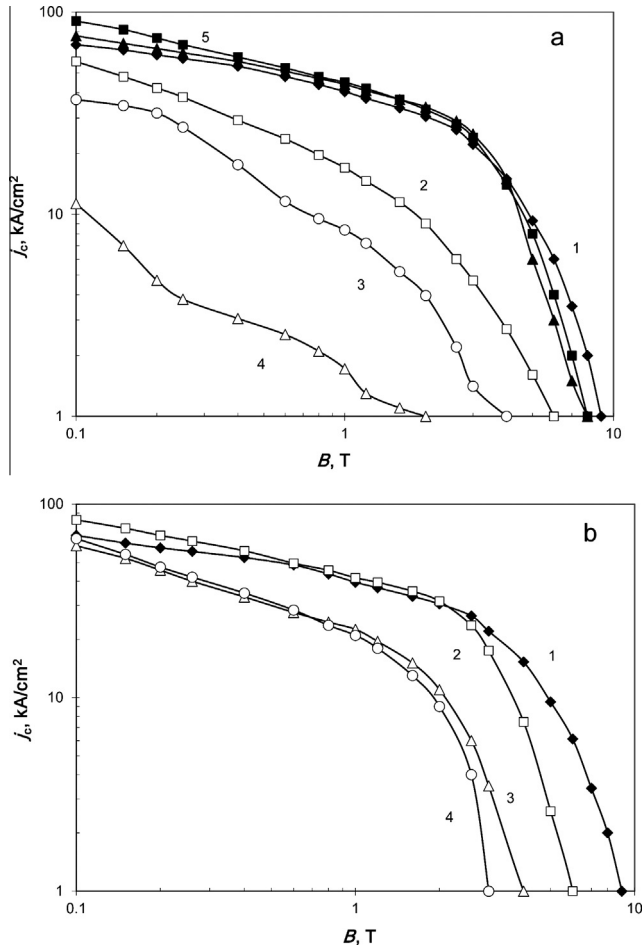


**Fig. 6.** Dependences of the critical current density on the external magnetic field parallel to the  $c$ -axis: after 200 °C annealing (a) and after two-staged annealing at 200 °C and at 930 °C followed by oxidation (b); 1 – initial state; 2 – with 0.22 wt.% H<sub>2</sub>O; 3 – with 0.36 wt.% H<sub>2</sub>O; 4 – with 0.63 wt.% H<sub>2</sub>O; 5 – after annealing at 200 °C for 18 h in oxygen atmosphere; 6 – aged for about 15 years.

phenomenon can be observed only in the single-crystals. As an illustration, Fig. 5 shows the YBa<sub>2</sub>Cu<sub>3</sub>O<sub>6.9</sub> single crystal, heat-treated in a humid argon atmosphere at a temperature of 200 °C. From this figure it becomes clear that the annealing for 20 h results in the stress fields in the matrix phase (four-petal figures) (Fig. 5b, highlighted with an oval). For longer annealing times, the number of defects and the related stress fields grows, with the twin-structure disappearing (Fig. 5c). The aging process of the single crystals is also responsible for the emergence of the stress fields. This is evidenced by the fact that under normal conditions, the water uptake gives rise to the formation of the stacking faults. (Fig. 5d, highlighted with an oval). From this micrograph it also follows that the water is absorbed unevenly. The single crystal is conventionally divided into two areas, one of which has the stress fields, and the second one retains the twin-structure. This fact is probably due to an uneven distribution of growth defects inside the single crystal. These are assumed to be the major reason for water penetration.

After recovery annealing at 930 °C, the dependencies  $j_c = f(C_{H_2O})$  for the samples absorbed water of  $\approx 0.2$  wt.% have maxima of  $j_c$ , with their values are above original ones by 30–100% (Fig. 3, curves 3, 4). The values of  $B_{c1}$  for these samples are also much greater than the initial (Fig. 4, curves 3, 4). This is a positive factor when it comes to practical applications of high temperature superconductors in devices running on alternating current [33].

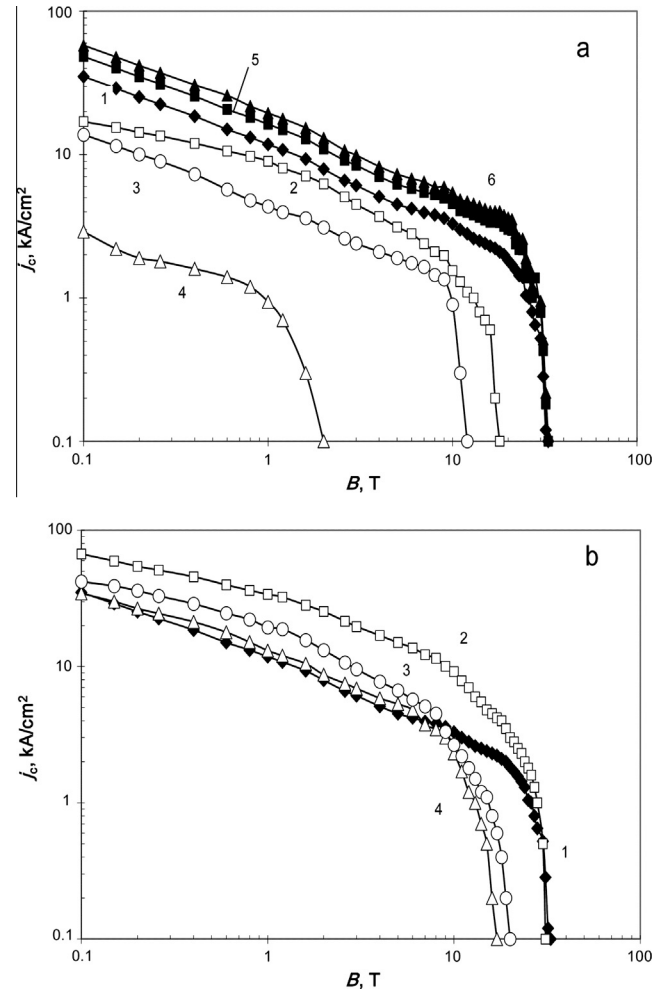


**Fig. 7.** Dependences of the critical current density on the external magnetic field perpendicular to the  $c$ -axis: after 200 °C annealing (a) and after two-staged annealing at 200 °C and at 930 °C followed by oxidation (b); 1 – initial state; 2 – with 0.22 wt.% H<sub>2</sub>O; 3 – with 0.36 wt.% H<sub>2</sub>O; 4 – with 0.63 wt.% H<sub>2</sub>O; 5 – after heat treatment at 200 °C for 18 h in oxygen atmosphere; 6 – aged for about 15 years.

The atmospheric composition for low temperature annealing affects essentially the dependencies  $j_c = f(B)$ . After the treatment of the samples in a dry oxygen atmosphere or after the natural aging process, these have a strong tendency to improve, especially in the field applied  $\perp c$ . (Figs. 6a and 7a). Conversely, during annealing at 200 °C in a humid argon atmosphere, the critical current density and the irreversibility field values ( $B_{irr}$ ) systematically drop as the samples absorb water.

After recovery annealing (930 °C) in the field applied parallel to the  $c$ -axis ( $\parallel c$ ), the values of  $j_c$  for the samples absorbed water of  $\leq 0.2$  wt.% go up against the initial state only in the low fields (Fig. 6b, curve 2). However, if the field is applied perpendicular to the  $c$ -axis ( $\perp c$ ), the critical current density  $j_c$  of the sample absorbed water of  $\sim 0.2$  wt.% rises dramatically in the high magnetic fields (Fig. 7b), with the values of  $B_{irr}$  reaching the initial. The values of  $j_c \geq 10^4$  A/cm<sup>2</sup> remain unchanged in the magnetic fields up to 10 T, which 5-fold exceeds the appropriate values for the initial sample.

The presence of water in the structure of YBa<sub>2</sub>Cu<sub>3</sub>O<sub>6.9</sub> yields a sharp drop of the pinning force in the case of applying the field parallel to the axis  $c$  (Figs. 8 and 9). If the field is applied perpendicular to the axis  $c$  ( $\perp c$ ), then two peaks at  $B \sim 6$  and  $B \sim 9$  T can be seen in the dependencies  $F_p = f(B)$  of the samples absorbed water (Fig. 9a, curve 2, indicated with arrows). Maximum at  $B \sim 6$  T

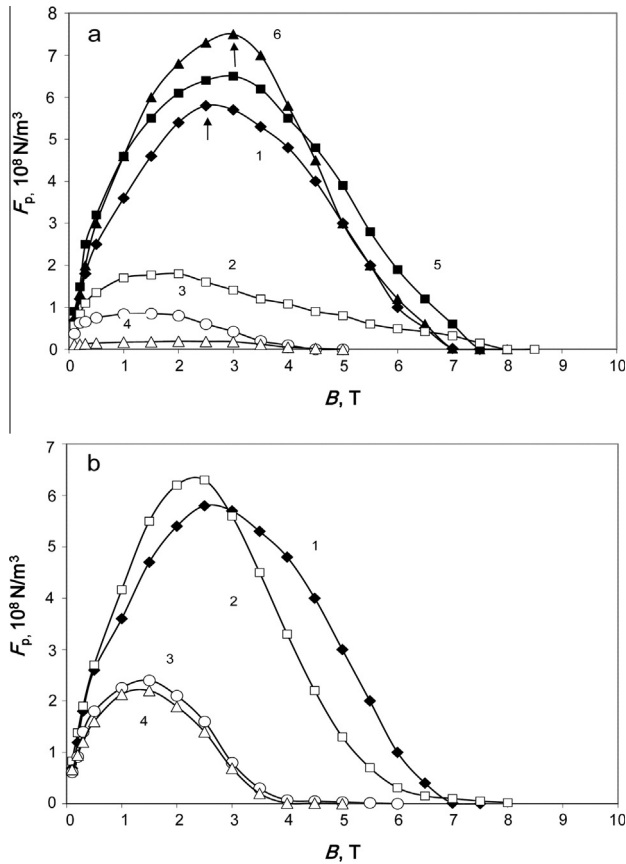


**Fig. 8.** Dependences of the pinning force  $F_p$  on the external magnetic field  $\parallel c$ : after 200 °C annealing (a) and after two-staged annealing at 200 °C and at 930 °C followed by oxidation (b): 1 – initial state; 2 – with 0.22 wt.%  $H_2O$ ; 3 – with 0.36 wt.%  $H_2O$ ; 4 – with 0.63 wt.%  $H_2O$ ; 5 – after heat treatment at 200 °C for 18 h in oxygen atmosphere; 6 – aged for about 15 years.

corresponds to the reduced field value  $h = B/B_{irr} \approx 0.2$ . This, according to the theory in Ref. [34], is characteristic of planar pinning centers, which are effective in the fields applied perpendicular to the axis  $c$  ( $\perp c$ ) [35].

In contrast, as for the samples treated in a dry oxygen atmosphere and aged under normal conditions, the pinning force increases. The peak of  $F_p$  shifts toward greater magnetic induction values (Figs. 8a and 9a, indicated by arrows). This proves the existence of nanoregions with quenched superconductivity. In the high magnetic fields, these manifest themselves as the pinning centers [2,36]. The particles precipitated in the phase with lower oxygen content may well be such pinning centers [11].

The recovery annealing of the samples absorbed water makes the maximum of the dependencies  $F_p = f(B)$  shift toward lower values of magnetic induction if the field is applied parallel to the  $c$ -axis ( $\parallel c$ ) (Fig. 8b). If the magnetic field is applied perpendicular to the  $c$ -axis ( $\perp c$ ), considerable growth of the pinning force (in the field up to 20 T) takes place only for the samples absorbed water of  $\approx 0.2$  wt.%. However, the maximum of  $F_p$  also shifts toward the lower fields (Fig. 9b, indicated by arrows). The increase in  $F_p$  happening mostly only in the field perpendicular to the  $c$ -axis attests to the fact that due to the multiple planar defects the correlated pinning takes place [2,36]. Further diminishing the pinning force  $F_p$  with increasing the amount of the absorbed water is a consequence of the formation of too much quantity of the defects.

The results obtained are in agreement with the magnetic susceptibility data. The samples absorbed water more than 1 wt.% exhibit virtually no superconductivity at  $T > 77$  K [15]. The

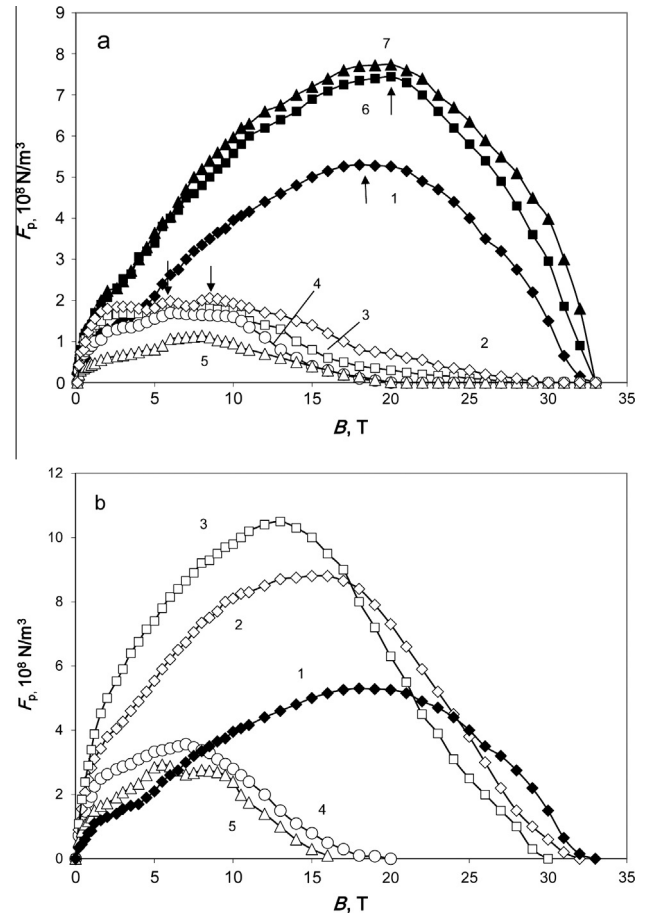


**Fig. 9.** Dependences of the pinning force  $F_p$  on the external magnetic field  $\perp c$ : after heat treatment at 200 °C (a) and after two-staged annealing at 200 °C and at 930 °C followed by oxidation (b): 1 – initial state; 2 – with 0.19 wt.%  $H_2O$ ; 3 – with 0.22 wt.%  $H_2O$ ; 4 – with 0.36 wt.%  $H_2O$ ; 5 – with 0.63 wt.%  $H_2O$ ; 6 – after heat treatment at 200 °C for 18 h in oxygen atmosphere; 7 – aged for about 15 years.

annealing at 930 °C (1 h) followed by oxidation restores the superconducting properties at the same temperature (Fig. 10, curves 2). However, there is a slight decrease in  $T_c$  from 92 to 88 K and the broadening of the transition to the superconducting state. Besides, the dependence  $\chi'' = f(T)$  has two peaks (Fig. 10b). One of them is associated with the transition of the bulk material to the superconducting state ( $T \sim 85$  K), and the second peak ( $T \sim 55$  K) is probably attributed to the transition of the regions that contain a large number of the remaining structural defects to the superconducting state.

For the sample absorbed water of  $\sim 0.2$  wt.%, the transition becomes broader, and the maximum of  $\chi'' = f(T)$  splits into twain (Fig. 10, curves 3). Apparently, both effects are due to the deterioration of superconductivity at the intergranular boundaries. Annealing at 930 °C and subsequent oxidation bring the sample properties back completely and the curves correspond to the initial state (Fig. 10, curves 4).

Fig. 11 presents the field dependencies of the ratio between  $j_c$  measured in the field parallel to  $c$  and  $j_c$  measured in the field applied perpendicular to  $c$  ( $j_c \parallel c / j_c \perp c$ ). This magnitude characterizes anisotropy of the material. The figure shows that this ratio rises significantly with the increase in the external field up to  $\sim 3$  T relative to the initial sample (Fig. 11a, curve 1). The samples aged and treated at 200 °C in an oxygen atmosphere have the same dependencies (Fig. 11a, curves 6, 7). In this case, the maximum position for  $B \sim 3$  T coincides with the maximum of the

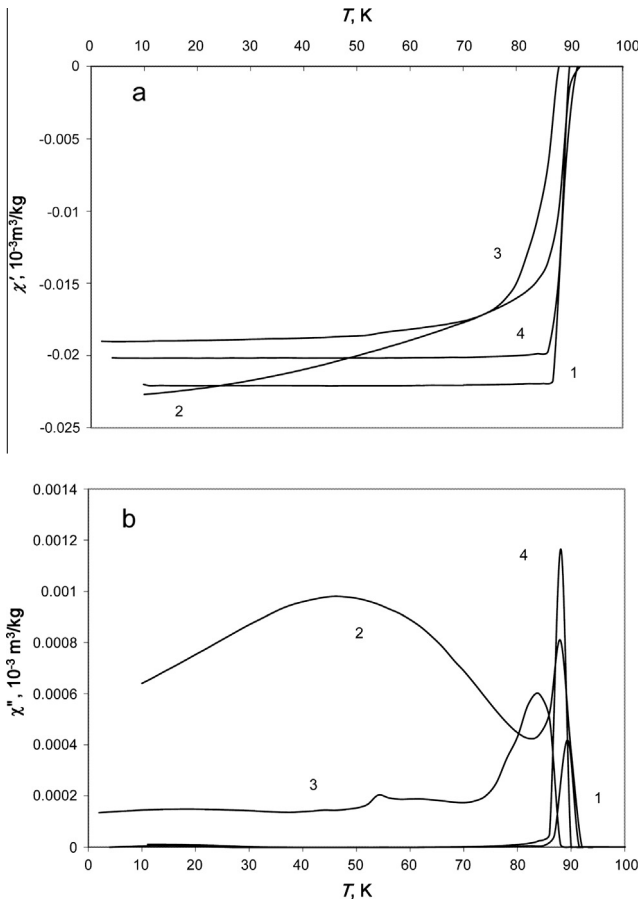


**Fig. 10.** Temperature dependences of magnetic susceptibility (a)  $\chi'$  and (b)  $\chi''$ : 1 – initial state; 2 – with 0.22 wt.% H<sub>2</sub>O; 3 – the sample, absorbed with >1 wt.% H<sub>2</sub>O at a temperature of 200 °C after annealing at 930 °C; 4 – the sample, absorbed with 0.22 wt.% H<sub>2</sub>O at a temperature of 200 °C after annealing at 930 °C.

$F_p = f(B)$ -dependence, subject to placing the samples in the field parallel to the  $c$ -axis ( $\parallel c$ ). This is explained by the fact that the critical current density  $j_c(\parallel c)$  drops slower than  $j_c(\perp c)$  as the external field becomes stronger. The pattern changes radically after treatment in an atmosphere saturated with water vapors. Then, a peak of the dependence  $j_c(\parallel c)/j_c(\perp c) = f(B)$  is observed without a magnetic field and the magnitude of the ratio  $j_c(\parallel c)/j_c(\perp c)$  is greater as compared with the initial state (Fig. 11a, curves 2–5).

After recovery annealing at 930 °C, the field dependencies of the ratio  $j_c(\parallel c)/j_c(\perp c)$  become like the original, but the maximum for  $B \sim 3$  T gradually disappears. (Fig. 11b, curves 2, 3). Under low temperature annealing, the sample absorbed water of  $\approx 0.22$  wt.% demonstrates an “almost isotropic” nature of the material ( $j_c(\parallel c)/j_c(\perp c) = 1$ ) in the fields up to  $\sim 3$  T ( $j_c(\parallel c)/j_c(\perp c) = 1$ ) (Fig. 11b, curve 4). This is caused by the fact that the critical current density  $j_c$  of the sample annealed at 930 °C increases considerably stronger in the field applied perpendicular to the  $c$ -axis ( $\perp c$ ) than in the field applied parallel to the  $c$ -axis ( $\parallel c$ ). If the water absorption exceeds 0.2 wt.%, the amount of the planar defects becomes too large and  $j_c(\parallel c) \neq j_c(\perp c)$  (Fig. 11b, curve 5).

According to the X-ray data, absorbing water, 123 transforms into the 124 type phase at least on the surface of the sample (Fig. 12, curve 2). This is consistent with the findings obtained for films [17,18]. In this case, the  $ab$ -plane still preserves a high texture. However, the lines become broad, which indicates the imperfection of the formed phase of 124-type. After the annealing at 930 °C, there is an inverse transition to the 123 phase. The samples absorbed water of  $\leq 0.36$  wt.% preserve the initial high texture.

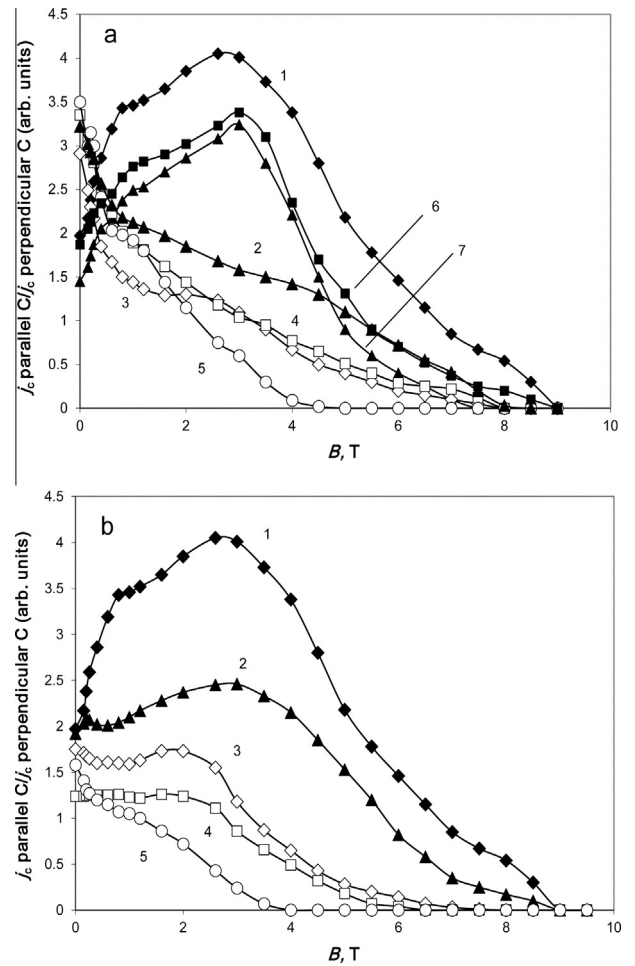


**Fig. 11.** The ratio of  $j_c(\parallel c)/j_c(\perp c)$  versus the external magnetic field: after 200 °C annealing (a) and after two-staged annealing at 200 °C and at 930 °C followed by oxidation (b): 1 – initial state; 2 – with 0.14 wt.% H<sub>2</sub>O; 3 – with 0.19 wt.% H<sub>2</sub>O; 4 – with 0.22 wt.% H<sub>2</sub>O; 5 – with 0.36 wt.% H<sub>2</sub>O; 6 – after 200 °C, 18 h annealing in oxygen atmosphere; 7 – aged for about 15 years.

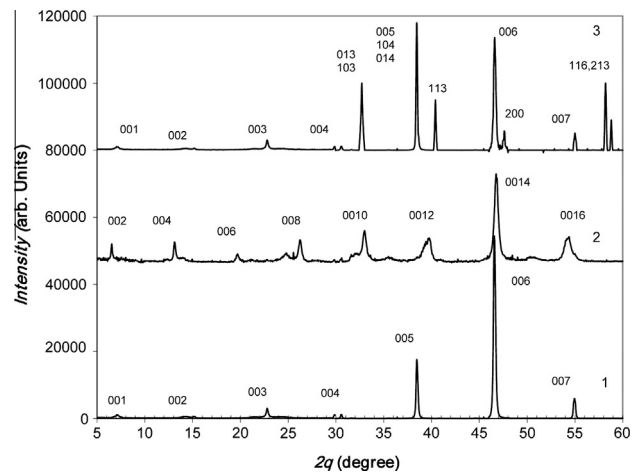


**Fig. 12.** X-ray diffraction patterns of YBa<sub>2</sub>Cu<sub>3</sub>O<sub>6.9</sub>: 1 – initial state (indices phase 123), 2 – intercalated with 0.29 wt.% H<sub>2</sub>O at 200 °C (indices phase 124), 3 – intercalated with 0.63 wt.% H<sub>2</sub>O at 200 °C and recovered by annealing at 930 °C followed by oxidation.

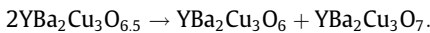
The latter is violated due to primary recrystallization only after the samples absorbed water of  $\geq 0.63$  wt.% have been restored (Fig. 12, curve 3). This is evidenced by the appearance of lines, inherent in

non-textured ceramics. Under these circumstances there is no improvement in the critical characteristics.

The samples annealed at 930 °C lose structural water; the atoms are largely arranged in an orderly manner because after oxidation, the 123-type passes into an orthorhombic lattice [23]. However, rhombic lattice distortion is weak, and the authors of [37], using the TEM-method, have observed an unusual system of twins (two twin-systems in planes (110) and (110), as well as a large number of dislocation clusters. The electron-diffraction pattern also shows weak orthorhombic distortion and a superposition of two reciprocal lattices. One of which belongs to the orthorhombic phase, and another – to the tetragonal phase, which speaks of the partial restoration of the original structure of 123, undergone the short-term annealing at 930 °C.

The above results indicate that the optimal amount of water to improve the  $\text{YBa}_2\text{Cu}_3\text{O}_{6.9}$  compound's electro-physical properties is ~0.2 wt.%. Then, it can be assumed that when absorbing the water, the available oxygen vacancies of  $\text{O}_1$ -type tend to be filled with  $\text{OH}^-$ -groups [38]. In addition to completing the oxygen vacancies, the formation of the stacking faults of the 124-type occurs [18]. However, a too large number of these defects impair the electro-physical properties. In particular, the excess of the planar defects can contribute to the magnetic field permeation and to a reduction of  $B_{c1}$  values provided that the field is applied perpendicular to the  $c$ -axis ( $\perp c$ ). Therefore, the distance between them in the  $ab$ -plane becomes smaller than the London penetration depth ( $\lambda \sim 140$  nm). In this case, the magnetic field permeates through the superconductor segments with an intact structure. Perhaps this is evidenced by the decrease in the values of  $B_{c1}$  for samples absorbed water of >0.2 wt.%.

As has been noted above, when annealed at a temperature of 200 °C in the oxygen atmosphere, the  $\text{YBa}_2\text{Cu}_3\text{O}_y$  ( $y \geq 6.5$ ) compound decomposes, absorbing practically no water. In this case, oxygen-depleted particles and oxygen-rich matrices are formed according to the scheme:



Similarly, when annealed in a humid neutral atmosphere, the  $\text{YBa}_2\text{Cu}_3\text{O}_y$  compound binds water, which results in forming the  $\text{YBa}_2\text{Cu}_3\text{O}_{7-2(\delta+x)}(\text{OH})_{2(\delta+x)}$  oxide hydroxide. If  $y \geq 0.5$ , the latter, in contrast to  $\text{YBa}_2\text{Cu}_3\text{O}_y$ , falls into the oxygen-rich matrix and oxygen-poor and water-rich particles according to following the reaction:



The particles of  $\text{YBa}_2\text{Cu}_3\text{O}_7$  are likely to be the stacking fault packets, which have been observed in [21].

Short-term recovery annealing (930 °C) partially retains the planar stacking faults and forms the non-equilibrium twin-system and dislocation clusters. [37] In the aggregate, all the structural defects (both endogenous and exogenous), being the pinning centers, appear to give rise to a synergistic effect, thereby essentially improving the current-carrying capacity of the material, double-annealed and absorbed the optimal amount of water. The deterioration of the critical characteristics after the recovery annealing of the samples absorbed water of >0.2 wt.% presumably occurs due to too high a density of the structural defects.

It should be noted that there is an analogy between the structures arising during the low temperature treatment and formed after high-energy particle irradiation. The increase in high-energy particle fluence as well as the annealing at a temperature of 200 °C in a humid atmosphere leads to the formation of the planar defects of the 124 type, a drastic reduction of anisotropy of  $j_c$ , and partial amorphization of the material [39–41].

It has been found [7] that the creation of two types of structural defects (point and columnar) essentially improves the critical parameters of the 123-type. Columnar defects provide large pinning energy but point ones prevent magnetic flux creep. It can be assumed that the combination of the columnar and planar defects, producing the pinning in the two directions ( $\parallel c$  and  $\perp c$ ), and the point defects can give a greater synergistic effect in enhancing the critical parameters and improving the isotropy of the electro-physical properties of a high-textured material.

#### 4. Conclusion

In the present article, it has been demonstrated that the structural defects (particles of the non-superconducting phase at  $T = 77$  K, stacking faults) formed during the low-temperature annealing have a profound positive effect on the critical characteristics of 123. Improvement of properties of the samples annealed at a temperature of 200 °C in a dry atmosphere is due to the precipitation of small oxygen-depleted particles, which produce the pinning of magnetic vortices. The introduction of water into the structure of  $\text{YBa}_2\text{Cu}_3\text{O}_{6.9}$  cuts down the critical current density  $j_c$ , however, at a certain water concentration (~0.1 to 0.2 wt.%), the values of  $B_{c1}$  noteworthy increase.

The short-term recovery annealing at 930 °C for 1 h and subsequent oxidation cause the critical current density for the samples absorbed water of ~0.2 wt.% as well as the magnitude of the first critical fields to grow significantly against the initial state. The most great increase in  $j_c$  and  $B_{c1}$  is observed in the magnetic field imposed perpendicular to the  $c$ -axis ( $\perp c$ ). This fact is accounted for by retaining the planar stacking faults of the 124-type after interaction with water. Despite the high texture, the material becomes more isotropic as regards the values of  $j_c$  in the fields up to ~3 T. The water content of ~0.2 wt.% in  $\text{YBa}_2\text{Cu}_3\text{O}_{6.9}$  before the recovery annealing is optimal.

The double treatment brings about larger values of the critical current density in high magnetic fields as compared to the treatment at 200 °C in a dry atmosphere when only phase decomposition occurs.

The optimal combination of the planar and columnar defects with microscopic inclusions of foreign phases is a necessary condition of getting a textured high-temperature-superconducting material, which would manifest practically isotropic properties and possess high-performance critical characteristics.

The effect of the low-temperature treatment in a wet environment is in a great measure similar to high-energy particle irradiation. As distinct from the latter, the low-temperature treatment is a much cheaper way to achieve high values of the critical parameters of advanced high-temperature superconducting materials like 123, which is extremely important for practical application.

#### Acknowledgments

We thank the workers of the Center of Collaborative Access, Institute of Metal Physics, Ural Branch, Russian Academy of Sciences, A.V. Korolev for performing the magnetic susceptibility measurements and V.A. Sazonov and M.V. Chuntunov for performing the XRD investigation.

The research was supported by the Project N 15-17-2-16 of the Ural Branch of the Russian Academy of Sciences.

#### References

- [1] Koblishka MR, Murakami M. *Supercond Sci Technol* 2000;13:738.
- [2] Muralidhar M, Murakami M. *Phys Rev B* 2000;62:13911.
- [3] Tretyakov YuD, Goodilin EA. *Physica B* 2002;321:249.

- [4] Selvamanchickam V, Yao Y, Chen Y, Shi T, Liu Y, Khatri ND, et al. *Supercond Sci Technol* 2012;25:125013. <http://dx.doi.org/10.1088/0953-2048/25/12/125013>.
- [5] Haugan T, Barnes PN, Wheeler R, Meisenkothen F, Sumption M. *Nature* 2004;430:967.
- [6] Matsumoto K, Mele P. *Supercond Sci Technol* 2010;23:014001.
- [7] Maiorov B, Baily SA, Zhou H, Ugurlu O, Kennison JA, Dowden PC, et al. *Nat Mater* 2009;8:398. <http://dx.doi.org/10.1038/NMAT2408>.
- [8] Varanasi C, Burke J, Wang H, Lee JH, Barnes P. *Appl Phys Lett* 2008;93:092501.
- [9] Harrington SA, Durrell JH, Maiorov B, Wang H, Wimbush SC, Kursumovic A, et al. *Supercond Sci Technol* 2009;22:022001.
- [10] Feldmann DM, Holesinger TG, Maiorov B, Foltyn SR, Coulter JY, Apodaca I. *Supercond Sci Technol* 2010;23:095004.
- [11] Daeumling M, Seuntjens JM, Labalestier DC. *Nature* 1990;346:332.
- [12] Kupfer HK, Kresse R, Meier-Hirmer R, Jahn W, Wolf T, Zhukov AA, et al. *Phys Rev B* 1995;52:7698.
- [13] Sudareva SV, Kuznetsova EI, Krinitsina TP, Bobylev IB, Romanov VNEP. *Physica C* 2000;331:263.
- [14] Bobylev IB, Sudareva SV, Zyuzeva NA, Krinitsina TP, Korolev AV, Blinova YuV, et al. *Phys Met Metallogr* 2004;98:288.
- [15] Bobylev IB, Zyuzeva NA. *Phys Solid State* 2013;55:930. <http://dx.doi.org/10.1134/S1063783413050053>.
- [16] Zhao Rupeng, Goringe MJ, Myhra S, Turner PS. *Philos Mag A* 1992;66:491.
- [17] Gunther W, Schollhorn R, Siegle H, Thomsen Ch. *Sol State Ionics* 1996;84:23.
- [18] Gunther W, Schollhorn R, Epple M, Siegle H, Thomsen Ch, Kabius B, et al. *Phyl Mag A* 1999;79:449.
- [19] Dooglav AV, Egorov AV, Mukhamedshin IR, Savincov AV, Alloul H, Bobroff J, et al. *Phys Rev B* 2004;70:054506-1.
- [20] Sudareva SV, Kuznetsov MV, Kuznetsova EI, Blinova YuV, Romanov EP, Bobylev IB. *Phys Met Metallogr* 2009;108:569. <http://dx.doi.org/10.1134/S0031918X09120072>.
- [21] Bobylev IB, Kuznetsova EI, Zyuzeva NA, Krinitsina TP, Sudareva SV, Romanov EP. *Phys Met Metallogr* 2010;110:378. <http://dx.doi.org/10.1134/S0031918X1010008X>.
- [22] Ponosov YuS, Bobylev IB, Zyuzeva NA. *JETP Lett* 2014;99:340. <http://dx.doi.org/10.1134/S0021364014060113>.
- [23] Bobylev IB, Zyuzeva NA, Romanov EP. *Phys Solid State* 2010;52:1338. <http://dx.doi.org/10.1134/S1063783410070024>.
- [24] Bobylev IB, Zyuzeva NA. *Phys Solid State* 2012;54:1332. <http://dx.doi.org/10.1134/S1063783412070074>.
- [25] Murakami M. *Supercond Sci Technol* 1992;5:185.
- [26] Murakami M, Sakai N, Higuchi T, Yoo SI. *Supercond Sci Technol* 1996;9:1015.
- [27] Zyuzeva NA, Bobylev IB. *Phys Met Metallogr* 2014;115:358. <http://dx.doi.org/10.1134/S0031918X14040176>.
- [28] Dorofeev G, Drobin V, Malinowski H. *J Phys: Conf Ser* 2014;507:012009.
- [29] Kano M, Kohama Y, Graf D, Balakirev FF, Sefat AS, McGuire MA, et al. *J Phys Soc Jpn* 2009;78:084719.
- [30] Kozłowski G, Maartense I, Spyker R, Leese R, Oberly CE. *Physica C* 1991;173:195.
- [31] Bobylev IB, Gerasimov EG, Zyuzeva NA. *Phys Solid State* 2012;54:1741.
- [32] Semenovskaya S, Khachatryan AG. *Phys Rev B* 1992;46:6511.
- [33] Blakemore JS. *Solid state physics*. Cambridge Univ. Press; 1988.
- [34] Dew-Hughes D. *Phil Mag* 1974;2:293.
- [35] Murakami M, Fujimoto H, Yamaguchi K, Nakamura N, Koshizuka N, Tanaka S. *Phase Trans* 1993;41:69.
- [36] Foltyn SR, Civalo L, MacManus-Driscoll JL, Jia QX, Maiorov B, Maley M, et al. *Nat Mater* 2007;6:631.
- [37] Bobylev IB, Kuznetsova EI, Krinitsina TP, Zyuzeva NA, Sudareva SV, Romanov EP. *Phys Met Metallogr* 2011;112:165. <http://dx.doi.org/10.1134/S0031918X11020177>.
- [38] Schougaard SB, Ali MF, McDevitt JT. *Appl Phys Lett* 2004;84:1144.
- [39] Zandbergen HW, Kulik J, Nieuwendij KB. *Physica C* 1991;179:43.
- [40] Sauerzopf FM, Wiesinger HP, Kritscha W, Weber HW, Crabtree, Liu JZ. *Phys Rev B* 1991;43:3091.
- [41] Goyal A, Kang S, Leonard KJ, Martin PM, Gapud AA, Varela M, et al. *Supercond Sci Technol* 2005;18:1533.